

LETTER TO THE EDITOR

***Herschel*^{*} PACS Spectroscopic Diagnostics of Local ULIRGs: Conditions and Kinematics in Mrk 231**

J. Fischer^{1, **}, E. Sturm², E. González-Alfonso³, J. Graciá-Carpio², S. Hailey-Dunsheath², A. Poglitsch², A. Contursi², D. Lutz², R. Genzel², A. Sternberg⁴, A. Verma⁵, and L. Tacconi²

¹ Naval Research Laboratory, Remote Sensing Division, 4555 Overlook Ave SW, Washington, DC 20375, USA
e-mail: jackie.fischer@nrl.navy.mil

² Max-Planck-Institut für extraterrestrische Physik (MPE), Postfach 1312, D-85741 Garching, Germany

³ Universidad de Alcalá de Henares, Departamento de Física, Campus Universitario, Spain

⁴ Sackler School of Physics and Astronomy, Tel Aviv University, Tel Aviv 69978, Israel

⁵ University of Oxford, Denys Wilkinson Building, Keble Road, Oxford OX1 3RH, United Kingdom

Received 31 March 2010; accepted 5 May 2010

ABSTRACT

In this first paper on the results of our *Herschel* PACS survey of local Ultraluminous Infrared Galaxies (ULIRGs), as part of our *SHINING* survey of local galaxies, we present far-infrared spectroscopy of Mrk 231, the most luminous of the local ULIRGs, and a type 1 broad absorption line AGN. For the first time in a ULIRG, all observed far-infrared fine-structure lines in the PACS range were detected and *all* were found to be deficient relative to the far infrared luminosity by 1 – 2 orders of magnitude compared with lower luminosity galaxies. The deficits are similar to those for the mid-infrared lines, with the most deficient lines showing high ionization potentials. Aged starbursts may account for part of the deficits, but partial covering of the highest excitation AGN powered regions may explain the remaining line deficits. A massive molecular outflow, discovered in OH and ¹⁸OH, showing outflow velocities out to at least 1400 km sec⁻¹, is a unique signature of the clearing out of the molecular disk that formed by dissipative collapse during the merger. The outflow is characterized by extremely high ratios of ¹⁸O / ¹⁶O suggestive of interstellar medium processing by advanced starbursts.

Key words. infrared: galaxies – galaxies: ISM – quasars: absorption lines – galaxies: individual: Mrk 231

1. Introduction

ULIRGs ($L_{IR} \geq 10^{12} L_{\odot}$), which in the local universe are known to be mergers of gas rich galaxies, are thought to play a critical role in galaxy evolution. It is therefore crucial to understand the conditions, dynamics, chemistry and energetics of this stage of evolution, in which dissipative collapse accompanies the transformation of gas rich galaxies into ellipticals (Lonsdale et al. 2006). As part of the *SHINING* Key Project on local galaxies, we are carrying out a far-infrared (FIR) spectroscopic survey of all 21 ULIRGs in the Revised Bright Galaxy Survey (Sanders et al. 2003). Previous work on ULIRGs with the Infrared Space Observatory (ISO) Long Wavelength Spectrometer (LWS) found deficits in far-infrared atomic and ionized fine-structure line emission relative to their FIR luminosities (Luhman et al. 1998) accompanied by prominent molecular absorption in excited transitions of molecules such as OH and H₂O rarely seen in other galaxies (Fischer et al. 1999). The deficits, often based only on a few non-detections, were postulated to result from the high ratios of UV radiation density to particle density in the nuclei of these galaxies (Malhotra et al. 2001, Luhman et al. 2003, Abel et al. 2009), high gas density (e.g. Negishi et al. 2001) and high FIR opacity and/or high luminosity-to-mass ratio

(González-Alfonso et al. 2004, 2008, hereafter GA04, GA08), but because of the paucity of diagnostic line detections this puzzle remained unresolved. GA04 and GA08 showed that the high excitation molecular absorptions in both Arp 220 and Mrk 231 are radiatively pumped, consistent with high radiation density to particle density. They identified far-infrared absorption by OH, H₂O, NH₃, NH, and ¹⁸OH, but the identifications of the latter species were uncertain due to the low resolution of the LWS. The PACS ULIRG spectroscopic survey is designed to kinematically identify the ionized, atomic and molecular regions and to study the conditions of the interstellar medium, thereby illuminating the nature of this important evolutionary phase. In this first paper we present our initial results on Mrk 231, the most luminous of the local ULIRGs ($L(8-1000 \mu m) = 3.2 \times 10^{12} L_{\odot}$) and a type 1, low-ionization broad absorption line (LoBAL) active galactic nucleus (AGN) at an adopted distance of 172 Mpc ($z=0.04217$). Its central quasar is covered by a semi-transparent dusty shroud producing about 3.1 magnitudes of extinction at 4400 Å (Reynolds et al. 2009) and is at the center of a rotating, nearly face-on molecular disk (Downes & Solomon 1998). Based primarily on *Spitzer* results, Veilleux et al. (2009) estimate that the average AGN contribution to the bolometric luminosity in ULIRGs is 35 – 40% and that for Mrk 231 the AGN contribution is ~ 70% by most estimation techniques. The contribution of an advanced 120 – 250 Myr nuclear starburst is estimated at 25 – 40% based on near infrared observations of Mrk 231 by Davies et al. (2007).

* *Herschel* is an ESA space observatory with science instruments provided by Principal Investigator consortia. It is open for proposals for observing time from the worldwide astronomical community.

** Visiting scientist at Max-Planck-Institut für extraterrestrische Physik (MPE), Garching, Germany

Table 1. Spectroscopic measurements for Mrk 231

Transition ^{a, b}	Line flux 10 ⁻¹⁷ W m ⁻²	Line flux error ^c 10 ⁻¹⁷ W m ⁻²	Equivalent Width 10 ⁻³ μm	Measured FWHM km s ⁻¹	Inferred FWHM ^d km s ⁻¹
[N III] 57.3 μm	2.8	0.6	-1.0	203	177
[O I] 63.2 μm	36.0	2.6	-17.0	232	218
[O III] 88.4 μm	4.1	0.6	-3.8	311	289
[N II] 121.9 μm	4.1	0.5	-10.4	389	266
[O I] 145.5 μm	3.2	0.4	-17.9	324	208
[C II] 157.7 μm	38.3	1.3	-296.0	337	247
[N II] 205.2 μm ^e	2.6	0.2	-61.0	524	242
OH 79.1, 79.2 μm	-22.8	1.0	15.3	—	—
	3.2	0.6	-2.1	—	—
OH 119.2, 119.4 μm	-47.6	0.3	107.4	—	—
	9.4	0.3	-21.6	—	—
¹⁸ OH 120.0, 120.2 μm	-14.7	0.2	34.3	—	—
	1.7	0.2	-4.0	—	—
H ₂ O 78.7 μm	-18.0	0.1	12.2	444	422
HF / H ₂ O 121.7 μm	-4.7	0.4	11.8	560	483

(^a) For doublets, fluxes listed are for the blended pair. (^b) For transitions with both absorption and emission, the absorption component is listed first. (^c) Errors listed are the statistical rms uncertainties; we allow 25% calibration uncertainties (see text). (^d) Inferred velocity width is based on the instrument resolution assuming a Gaussian profile; FWHMs are not listed for doublets. (^e) *Herschel* SPIRE data (V10).

2. Observations and data reduction

The observations were taken with the Photodetector Array Camera and Spectrometer (PACS) integral field spectrometer (Poglitsch et al. 2010) on board the *Herschel* Space Observatory (Pilbratt et al. 2010) in high spectral sampling range spectroscopy mode using small chop-nod cycles. Scans covering the range ± 1300 km s⁻¹ were taken around five fine-structure lines and a longer range scan included the OH 119 μm ²Π_{3/2} 5/2 – 3/2 Λ-doublet transitions, the ¹⁸OH 120 μm counterparts, and the [NII] 122 μm fine-structure line. The OH 79 μm ²Π_{1/2} – ²Π_{3/2} 1/2 – 3/2 Λ-doublet transitions, the nearly superposed ¹⁸OH counterparts, and the H₂O 78.7 μm 4₂₃ – 3₁₂ line were observed in parallel on the blue array.

The basic data reduction was done using the standard PACS reduction and calibration pipeline (ipipe) included in HIPE 2.0 1340¹. The data are consistent with an unresolved point source. For a well centered point source, the peak line and continuum flux will fall on the central of the PACS 5 x 5 spaxels (9'' x 9'' spatial pixels), with nearly all of the rest of the flux falling on the remaining pixels of the array. The best signal-to-noise on a faint line is obtained by scaling the line profile on the central spaxel, to the continuum flux integrated over the array. Where better baselines were obtained by scaling the sum of the brightest spaxels, this was done instead. For the [CII]158 μm scan, all of the spaxels were co-added.

At the time of preparation of this paper the full planned calibration procedure is not yet incorporated into the pipeline. For calibration of the PACS line fluxes, the line scan continua were therefore scaled to a fit to existing photometry of Mrk 231. The integrated line fluxes, statistical errors, equivalent widths, measured Gaussian-fit Δv_{FWHM} and the inferred intrinsic Δv_{FWHM} obtained by subtracting the instrumental Δv_{FWHM} in quadrature are listed in Table 1. We note that the [CII], [OI]63, and OH119 line fluxes are in agreement with ISO LWS line fluxes reported in Luhman et al. (2003) and GA08 to within the statistical uncertainties, but the stronger [NII] line flux reported in GA08 is not consistent with our observations. Additionally the [N II] 205

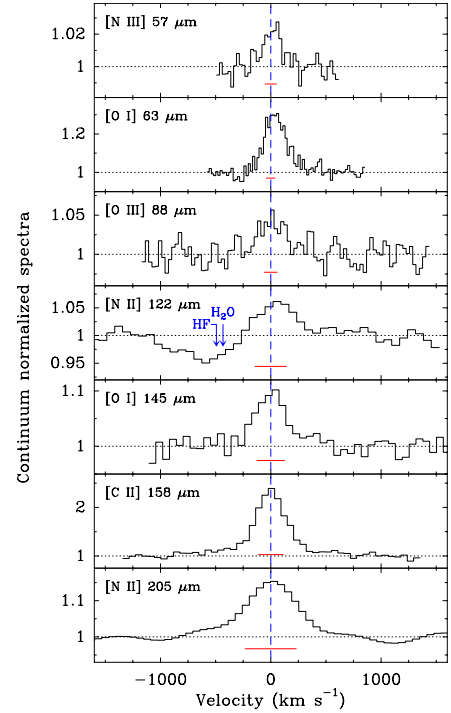


Fig. 1. Mrk 231 normalized far-infrared fine-structure line profiles versus velocity. The red bars represent the instrumental FWHMs. The absorption observed to the blue side of the [NII]122 μm line is due to the HF 2-1 and/or H₂O 4₃₂ – 4₂₃ lines.

μm line measured by *Herschel* SPIRE is included in Table 1 and Fig. 1 based on measurements presented in van der Werf et al. (2010, hereafter V10). We estimate the calibration uncertainties to be $\pm 25\%$.

3. Results and Discussion

3.1. The fine-structure lines

The continuum normalized fine-structure line spectra are displayed in Fig. 1 as a function of velocity, where Mrk 231's red-

¹ HIPE is a joint development by the *Herschel* Science Ground Segment Consortium, consisting of ESA, the NASA *Herschel* Science Center, and the HIFI, PACS and SPIRE consortia.

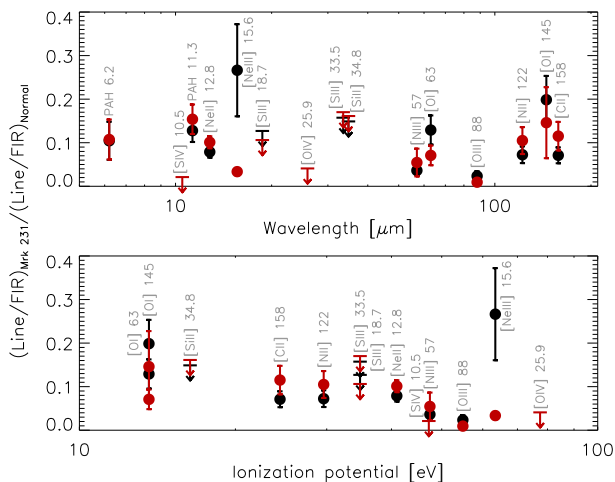


Fig. 2. Line-to-FIR ratio in Mrk 231 divided by the median line-to-FIR ratio in a sample of HII galaxies (black symbols) and AGN (red symbols) versus wavelength (*top*) and ionization potential (*bottom*). The mid-infrared line fluxes in Mrk 231 are from Armus et al. (2007). The error bars include the Mrk 231 calibration uncertainties and the statistical errors for the comparison sample values.

shift of 0.04217 is defined as 0 km s^{-1} and the red horizontal bars represent the instrumental FWHMs. The FWHM velocities observed in these lines are in all cases larger than the instrumental resolution and we do not detect self-absorption. The average of the derived intrinsic FWHMs for the fine-structure lines is 235 km s^{-1} , similar to the FWHM velocity widths of 167 km s^{-1} and 270 km s^{-1} measured by Sanders et al. (1991) and Tacconi et al. (2002) from CO(1–0) and near-infrared stellar CO band-head studies, respectively. Thus the fine-structure line emission is probably associated with the central star forming disk. In the [CII] line, wings not characteristic of the instrumental profile are present, out to -1000 km s^{-1} for the blue wing, suggesting that some C^+ is associated with the outflow discussed in the next subsection. The [NII]205 profile also suggests a wing out to -700 km s^{-1} , consistent with the detection of optical [NII] lines by Rupke et al. (2005). We estimate that the absorption by HF or H_2O observed in the blue wing of the [NII] $122 \mu\text{m}$ line does not affect the [NII] line flux by more than 50%, since the FWHM of this transition is similar to those of the other fine-structure lines. The observed [NII]205 to [NII]122 ratio of 0.6 ± 0.4 translates into a density range for N^+ of $\log n_e = 1.4^{+0.8}_{-0.4}$ (Rubin et al. 1993). Photodissociation region (PDR) modeling of [CII], [OI], and FIR fluxes yields UV radiation field and density $G_0 \approx 6 \times 10^3$ and $n \approx 500 \text{ cm}^{-3}$, at the extreme range of average radiation density per particle density seen in extragalactic nuclei (Sturm et al. 2010, Fig. 4).

The fine-structure line strengths relative to the far-infrared luminosities are weak compared with normal HII galaxies and AGN. In Fig. 2, we plot as a function of wavelength (top) and ionization potential (bottom) the fine-structure line to far-infrared flux ratio (FIR, 42 – 122 μm) in Mrk 231 relative to the median value for subsamples of HII galaxies (black symbols) and AGN (red symbols) with luminosities $1 \times 10^9 L_{\odot} \leq L_{\text{IR}} \leq 5 \times 10^{11} L_{\odot}$ and major isophotal diameters $D_{25} \leq 250$ arcsecs compiled from the literature and our *SHINING* sample (Graciá-Carpio et al., in prep.). There are no [NII] 205 μm line measurements for the comparison samples, so this line is not included in Fig. 2. The observed deficits are severe: typically an order of

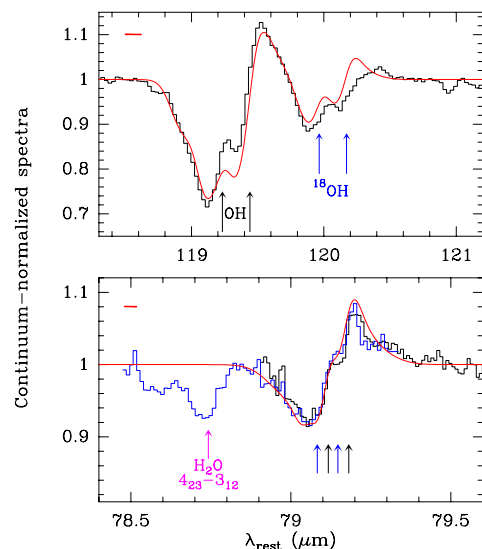


Fig. 3. P-Cygni profiles (solid blue, black histograms) of the OH 119 μm and ^{18}OH 120 μm partially resolved doublets (*top*) and the OH 79 μm unresolved doublet (*bottom*) in Mrk 231 are compared with our modeled profiles (solid red curves, see text). Absorption in the H_2O 4₂₃ – 3₁₂ transition with a possible blue-shifted wing is modeled in GA10. The zero velocity rest-frame wavelengths are marked with black (OH), blue (^{18}OH), and magenta (H_2O) arrows and the instrumental FWHM is indicated in each panel with horizontal red bars.

magnitude for the neutral and low ionization species and up to two orders of magnitude for the higher ionization lines. There is no correlation between the deficit and wavelength, and only weak correlation with critical density, so *differential* extinction (with wavelength) does not appear to play a significant role, and density does not play a major role. We find a strong inverse correlation (correlation coefficient, -0.78) with ionization potential when compared with the AGN sample. A similar inverse correlation is found with the starburst comparison sample only if the [NeIII]15 deficit is treated as an outlier. Low excitation is consistent with the estimation by Davies et al. (2007) that a 120 – 250 Myr starburst supplies 25 – 40 % of the bolometric luminosity of Mrk 231. However such an aging starburst can create a deficit of 40% at most. The high relative strength of the [OI] 145 μ m line, with its high excitation lower level, is suggestive of increased radiation density per particle density, as parameterized by the ionization parameter U (Luhman et al. 2003; Abel et al. 2009). The high ratio [OI] 145 / [CII] 158 $\approx 1/11$ lies between the predicted line ratio for starburst and AGN at the far-infrared F(60)/F(100) color of Mrk 231 with $U \approx 10^{-2}$ (high U) in the dust-bounded models of Abel et al. (2009). The strong inverse correlation relative to the AGN comparison sample in Fig. 2 is consistent with partial covering, higher for high ionization lines, of the line emitting region, due for example to a face-on molecular torus, with optically thick clumps.

3.2. The molecular outflow

Figure 3 displays the observed $119 - 120 \mu\text{m}$ OH / ^{18}OH and $79 \mu\text{m}$ H_2O / OH line profiles in Mrk 231. The OH lines show spectacular P-Cygni profiles in all three ground-state doublets, with extremely broad blue-shifted absorption as far out as 1400 km s^{-1} in the OH $119 \mu\text{m}$ line. Both the high *molecular* out-flow velocities and the relative strengths of the OH and ^{18}OH

are unprecedented. The excited H_2O $78.7\ \mu\text{m}$ and $\text{HF}/\text{H}_2\text{O}$ $121.7\ \mu\text{m}$ lines (see Fig. 1) appear to have blue-shifted wings, indicating that H_2O and HF may also be involved in the outflow. Recently a molecular outflow was detected by Sakamoto et al. (2009) in submillimeter lines of HCO^+ and CO toward the nuclei of Arp220 with an outflow velocity of $\sim 100\ \text{km s}^{-1}$, but this is modest compared with that of Mrk 231.

Our model of the observed profiles is shown in Fig. 3 and is based on the continuum components and radiative pumping described in González-Alfonso et al. (2010, hereafter GA10). It uses three continuum components, hot (radius = 23 pc, $T_{\text{dust}} = 400 - 150\ \text{K}$), warm (120 pc, 95 K), and extended (610 pc, 41 K), and three velocity components at 100, 400, and $600\ \text{km s}^{-1}$ (the latter component with high turbulent velocity, $300\ \text{km s}^{-1}$). We have conservatively assumed a screen approach for OH, with the outflow located just around the warm continuum source, resulting in $N(\text{OH}) = 1.4 \times 10^{17}\ \text{cm}^{-2}$. The model indicates mechanical energy $\gtrsim 10^{56}\ \text{erg}$ (dominated by the high velocity component), mechanical luminosity $\gtrsim 1\%$ of the TIR luminosity, and an outflow mass of $\gtrsim 7 \times 10^7\ M_{\odot}$. Observations of high-lying OH lines would help better constrain the outflow location, energetics, and the apparent extremely low $^{16}\text{O}/^{18}\text{O}$ ratio.

Figure 4 (top) shows that the absorption at $120\ \mu\text{m}$ by ^{18}OH at low outflow velocities ($> -250\ \text{km s}^{-1}$) is deeper than the corresponding absorption in the cross-ladder $79\ \mu\text{m}$ OH doublet at the same velocity. In this simple model we assume that the incomplete absorption in the optically thick OH $119\ \mu\text{m}$ doublet is a result of the fact that OH at a given velocity is only covering a fraction of the continuum (Fig. 4, middle) and we ignore any differential re-emission of the ^{18}OH and $79\ \mu\text{m}$ OH lines. We infer that at velocities $> -250\ \text{km s}^{-1}$ $\tau_{\nu}(^{18}\text{OH } 120\ \mu\text{m}) > \tau_{\nu}(\text{OH } 79\ \mu\text{m})$ (Fig. 4, bottom). From the ratio of the Einstein B coefficients, we find that the opacity in the $79\ \mu\text{m}$ OH line is 40 times lower than in the $119\ \mu\text{m}$ OH line and thus that $N(\text{OH})/N(^{18}\text{OH}) < 40$. These results are not critically dependent on the uncertainties in the covering factor due to re-emission (or thermal emission) in the $119\ \mu\text{m}$ OH line, which would affect both the opacities of the ^{18}OH and $79\ \mu\text{m}$ OH lines but not their relationship. We note that the effects of filling in by cooler dust would weaken the $120\ \mu\text{m}$ absorption more than the $79\ \mu\text{m}$ absorption. The rarer isotopologue ^{17}OH would appear between the two lines at 119 and $120\ \mu\text{m}$, but it is not possible to put a limit on its strength due to the broad width of the detected features.

We note that CH^+ , HCl , H^{37}Cl , H^{79}Br , and H^{81}Br have transitions at $\approx 120\ \mu\text{m}$, but HCl and HBr and their isotopologues are not expected to significantly contaminate the observed absorption due to the high lower level energies of their $120\ \mu\text{m}$ transitions (180–240 K). On the other hand, $\text{CH}^+(3-2)$ at $119.86\ \mu\text{m}$ could significantly contaminate the blue-shifted component of the ^{18}OH doublet, given that $\text{CH}^+(1-0)$ is detected in Mrk 231 (V10). We estimate that contamination by CH^+ could decrease the implied ^{18}OH abundance by a factor of 1.5 – 2 and the $^{16}\text{O}/^{18}\text{O}$ ratio could be increased to $\sim 30 - 40$, still significantly below the solar system isotopic ratio of 500, the galactic center ratio of 250, the starburst galaxy ratio of ~ 150 , and very close to the enhancement to ~ 50 that is theoretically predicted with a top heavy initial mass function in an advanced starburst stage (Henkel & Mauersberger 1993). If our simple model is correct, the high $^{18}\text{O}/^{16}\text{O}$ ratio seen here provides stringent constraints for stellar nucleosynthesis models.

Rupke et al. (2005) find that although both AGN and starburst galaxies have massive outflows traced by broad interstellar Na I D absorption lines, the high velocity ($\Delta v \geq 2000\ \text{km}$

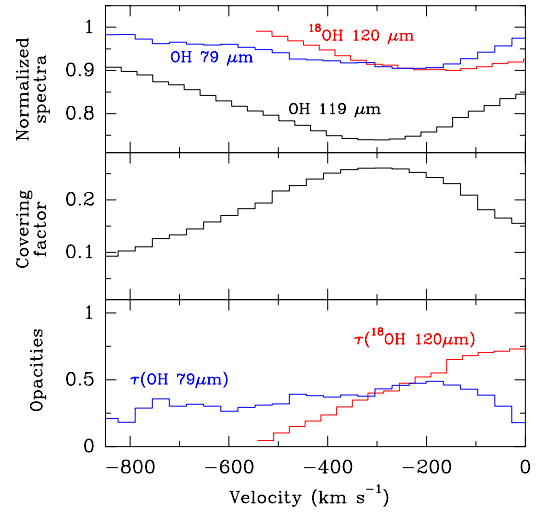


Fig. 4. Normalized velocity profiles for the blue-shifted OH and ^{18}OH absorption (top). The velocity scale is given relative to the bluest component of each OH doublet. The covering factor (middle), assumed to be the same for OH and ^{18}OH and derived from the profile of the optically thick OH $119\ \mu\text{m}$ line, is used to calculate the opacities in the $79\ \mu\text{m}$ and $120\ \mu\text{m}$ lines (bottom, see text).

s^{-1}) outflows seen almost exclusively in type 1 ULIRGs including Mrk 231, are probably powered by the AGN. This was also shown in models by Narayanan et al. (2008). If it is also true for the massive and energetic moderate velocity outflow seen here for the first time in OH and ^{18}OH , then an AGN driven outflow is in the process of dispersing into the intergalactic medium, highly processed material produced by an advanced starburst. The molecular outflow shows velocities similar to the kiloparsec scale outflow component of Mrk 231 seen by Rupke et al. and appears to be a unique signature of the clearing out of the molecular disk that formed with the dissipative collapse during the merger.

Acknowledgements. PACS has been developed by a consortium of institutes led by MPE (Germany) and including UVIE (Austria); KU Leuven, CSL, IMEC (Belgium); CEA, LAM (France); MPIA (Germany); INAF-IFSI/OAA/OAP/OAT, LENS, SISSA (Italy); IAC (Spain). This development has been supported by the funding agencies BMVIT (Austria), ESA-PRODEX (Belgium), CEA/CNES (France), DLR (Germany), ASI/INAF (Italy), and CICYT/MCYT (Spain). We thank the HerCULES Key Project for providing the [NII] $205\ \mu\text{m}$ profile. Basic research in IR astronomy at NRL is funded by the US ONR. JF acknowledges support from the NHSC and wishes to thank MPE for its hospitality during the first exciting year of *Herschel* science.

References

- Abel, N., Dudley, C., Fischer, J., Satyapal, S., van Hoof, P. 2009, *ApJ*, 701, 1147
- Armus, L., Charmandaris, V., Bernard-Salas, J., et al. 2007, *ApJ*, 656, 148
- Davies, R., Mueller Sánchez, F., Genzel, R. et al. 2007, *ApJ*, 671, 1388
- Downes, D. & Solomon, P. 1998, *ApJ*, 507, 615
- Fischer, J., Luhman, M., Satyapal, S., et al. 1999, *Ap&SS*, 266, 91
- González-Alfonso, E., Smith, H., Fischer, J., et al. 2004, *ApJ*, 613, 247 (GA04)
- González-Alfonso, E., et al. 2008, *ApJ*, 675, 303 (GA08)
- González-Alfonso, E., et al. 2010, *A&A*, this issue (GA10)
- Henkel, C. & Mauersberger, R. 1993 *A&A*, 274, 730
- Lonsdale, C., Farrah, D., Smith, H. 2006, *Astrophysics Update 2*, ed. J. Mason. (Springer Verlag, Heidelberg) 285
- Luhman, M., Satyapal, S., Fischer, J. et al. 1998, *ApJL*, 204, 11
- Luhman, M., Satyapal, S., Fischer, J., et al. 2003, *ApJ*, 594, 758
- Malhotra, S., Kaufman, M., Hollenbach, D., et al. 2001, *ApJ*, 561, 766
- Narayanan, D., Cox, T., Kelly, B., Davé, B., et al. 2008, *ApJ*, 176, 331
- Negishi, T., Onaka, T., Chan, K.-W., Roellig, T. 2001, *A&A*, 375, 566

- Pilbratt, G., et al. 2010, A&A, this issue
Poglitsch, A., et al. 2010, A&A, this issue
Reynolds, C., Punsly, B., Kharb, P. 2009, ApJ, 706, 851
Rubin, R., Simpson, J., Lord, S., et al. 1994, ApJ, 420, 772
Rupke, D., Veilleux, S., & Sanders, D. 2005 ApJ, 632, 751
Sakamoto, K., Aalto, S., Wilner, D. et al. 2009, ApJL, 700, 104
Sanders, D., Scoville, N., & Soifer, B. 1991, ApJ, 370, 158
Sanders, D., Mazzarella, J., Kim, D.-C. 2003, AJ, 126, 1607
Sturm, E., Verma, A., Graciá-Carpio, J. et al. 2010, A&A, this issue
Tacconi, L., Genzel, R., Lutz, D. et al. 2002, ApJ, 580, 73
van der Werf, P., et al. 2010, A&A, this issue (V10)